

# Atomic step motion during the dewetting of ultra-thin films

O. Pierre-Louis<sup>1,2</sup>, A. Chame<sup>3</sup>, M. Dufay<sup>1,2</sup>

<sup>1</sup> LPMCN, Université Lyon 1, 43 Bd du 11 novembre, 69622 Villeurbanne, France.

<sup>2</sup> Laboratoire de Spectrométrie Physique, UJF Grenoble 1, BP 87, 38402 St Martin d'Hères, France.

<sup>3</sup> Universidade Federal Fluminense, Avenida Litorânea s/n, 24210-340 Niterói RJ, Brazil

(Dated: November 7, 2018)

We report on three key processes involving atomic step motion during the dewetting of thin solid films: (i) the growth of an isolated island nucleated far from a hole, (ii) the spreading of a monolayer rim, and (iii) the zipping of a monolayer island along a straight dewetting front. Kinetic Monte Carlo results are in good agreement with simple analytical models assuming diffusion-limited dynamics.

## I. INTRODUCTION

The shape changes of crystals are usually governed by the motion of atomic steps at the surface<sup>1,2</sup>. The study of steps dynamics have permitted a better understanding of the morphological changes during various non-equilibrium processes, such as crystal growth<sup>1</sup>, surface electromigration<sup>1</sup>, or the decay of performed structures<sup>3</sup>. In the present paper, we focus on some key processes involving the dynamics of atomic steps during the dewetting of ultra-thin solid films. Dewetting is the process by which a continuous film breaks down into islands to lower the global energy. A large body of theoretical work has been devoted to the dynamics of dewetting with various continuum models<sup>4-9</sup>. Nevertheless, Kinetic Monte Carlo (KMC) simulations<sup>10,11</sup> have revealed that the dewetting process is controlled by the nucleation and dynamics of atomic steps on facets. Furthermore, recent studies have reported the observation of facets in dewetting experiments with Ag/Si(111)<sup>12</sup>, SOI (Si/SiO<sub>2</sub>) systems<sup>13,14</sup>, and YBaCuO films<sup>15</sup>, hence suggesting that atomic steps could play a crucial role in the dynamics.

A full analysis of the morphological evolution during dewetting would require to investigate not only step motion, but also the formation of new steps via two-dimensional nucleation. Such an approach was proposed recently in Refs.<sup>10,11</sup>. However, a quantitative description of nucleation is in general delicate because it requires an accurate determination of the step free energy which enters in the nucleation barrier. We shall here discard the nucleation process, and focus on the motion of steps in various geometries.

The paper is organized as follows. In section II, we provide a description of the KMC model. Section III focuses on the layer-by-layer dewetting regime. In this regime, an island is first nucleated far from a pre-existing hole in the film. The island then grows by diffusion-limited mass transfer from the hole. We shall here present an analytical solution of the island growth process, which provides a good agreement with the KMC simulations. The island finally grows so much that it surrounds the hole, and forms a monolayer 'rim' around it. In section IV, we provide an expression for the dynamics of the monolayer rim once it has surrounded the hole. This expression is in quantitative agreement with the simulations, and con-

tains some logarithmic corrections as compared to the simple linear behavior proposed in Ref<sup>11</sup>. In section V, we consider a different regime where a thick faceted rim forms during the dewetting process. Islands nucleated on the rim facet then grow in size and spread along the dewetting front with a well defined velocity  $V_{zip}$ . The numerical evaluation of this velocity is difficult because it would require delicate front-tracking procedures. We therefore present a method which allows one to determine this velocity from a single snapshot of KMC simulations. This method, the results of which were presented in Ref.<sup>11</sup>, is reported here in details.

## II. KMC SIMULATIONS

We model the dewetting of a crystalline film using a solid-on-solid model on a 2D square lattice. The lattice unit is  $a$ . The substrate surface is perfectly flat and frozen. The local height is  $z$ . On the epilayer atoms  $z > 0$ , and on the substrate  $z = 0$ .

We employ KMC simulations to implement the dynamics. Epilayer atoms hop to nearest neighbor sites with rates  $r_n$  when they are in contact with the substrate ( $z = 1$ ), and  $\nu_n$  when they are not in direct contact with the substrate ( $z > 1$ ). In our model, an atom needs to break all its bonds to hop. The hopping barrier is therefore given by the binding energy of the atom. Hence:

$$r_n = \nu_0 e^{-nJ/T + E_S/T} \quad (1)$$

$$\nu_n = \nu_0 e^{-nJ/T} \quad (2)$$

where  $\nu_0$  is an attempt frequency,  $T$  is the temperature (in units with  $k_B = 1$ ),  $n$  is the number of in-plane nearest neighbors of the atom before the hop,  $J$  is the bond energy, and  $E_S$  is the adsorbate-substrate excess energy. The model is presented in Fig1. Note that we do not write explicitly the bond  $J$  between the moving atom and the atom directly underneath it in the energy barrier for atom motion in Eqs.(1,2). Indeed, since this bond is present below any atom before the hopping event, we rather include its contribution  $\exp[-J/T]$  in the prefactor  $\nu_0$ . We choose  $J$  as the energy unit, so that  $J = 1$  in the following.

The algorithm used in the simulations is the following. We list all atoms into classes. Each class is characterized

by the number of in-plane neighbors  $n$  of the atom and by the existence or not of a nearest neighbor belonging to the substrate. At a given time  $t$ , we calculate the probabilities per unit time  $w_i$  of all possible events ( an event is the motion of an atom originally at position  $i$  ) given either by Eq.(1) or Eq.(2), and the sum  $W$  of all those rates (for all mobile atoms). We increment the time by a  $\delta t$ , which is equal to the inverse of the sum of the rates of all possible events,  $1/W$ . This choice for  $\delta t$  corresponds to the average value of the waiting time between two successive events (Poisson processes)<sup>16</sup>. We choose the event with probability  $w_i/W$ . The chosen atom moves with equal probability in any of the four possible directions.

The parameter  $E_S$  controls the wetting properties of the film on the substrate. In order to relate more precisely  $E_S$  to surface energetics, let us perform two Gedankenexperiments. The first one consist in splitting an epilayer crystal into two parts perpendicular to the  $z$  axis. We obtain two surfaces, and the energy balance is:  $J = 2E_{AV}$ , where  $E_{AV}$  is the energy per site of the created facet. The second Gedankenexperiment is to separate the substrate and the epilayer. The energy balance now reads:  $E_{AS} + J - E_S = E_{AV} + E_{SV}$ , where  $E_{AS}$  and  $E_{SV}$  is the epilayer-substrate and substrate-vacuum energies per lattice site. Combining these two relations, we find

$$E_S = E_{AV} + E_{AS} - E_{SV}. \quad (3)$$

Since the simulations were performed at a fixed temperature  $T$ , we should in principle consider a balance between free energies, rather than energies. However, since the substrate is frozen, the epilayer-substrate, and substrate-vacuum interfaces do not exhibit any configurational entropy. Their energy is therefore equal to their free energy. In addition we will work below the roughening temperature, so that the epilayer-vacuum free energy can also be approximated by an energy. As a consequence, the parameter  $E_S$  is, to a good approximation, a balance of free energies. This parameter is then identical (with opposite sign) to the thermodynamic work of adhesion  $S$  defined in Ref.<sup>17,18</sup>.

When  $E_S \leq 0$ , we have complete wetting. The regime of partial wetting is obtained for  $E_S > 0$ . At low temperatures, the equilibrium island shape has a square base of lateral size  $L_{eq}$ , and a height  $h_{eq}$ , with  $h_{eq}/L_{eq} = E_S$ . When  $E_S \gg 1$ , the energy minimization will favor high islands. As  $E_S$  is decreased to lower values, the equilibrium aspect ratio of the island decreases, and the islands become flat for  $E_S \ll 1$ .

### III. ISLAND AND HOLE GEOMETRY

#### A. Model

Let us consider the dewetting process starting from a pre-existing hole in a film of thickness  $h$ . Such a process

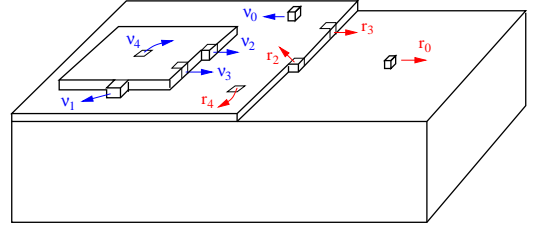


FIG. 1: Kinetic Monte Carlo (KMC) model, with hopping rates  $r_n$  and  $\nu_n$ .

mimics dewetting initiated at heterogeneous nucleation sites. When  $E_S$  is small or  $h$  is large, dewetting occurs in a layer-by-layer fashion. The precise criterion for this regime to occur was given in Ref.<sup>11</sup>. The process starts with the nucleation of a monolayer island on the film. Since this nucleation event is randomly located<sup>11</sup>, the island-hole distance is usually large, as shown in Fig.2(b). The island and the hole then grow simultaneously due to mass transfer from the hole to the island. We shall here focus on this island and hole growth process, and propose an analytical expression for the dynamics. We assume that the hole-island pair is isolated on the surface: no other hole or island exists in its neighborhood. In the initial stages, the distance between the hole and the island is larger than the typical sizes of the hole and the island. In this limit, we may assume that the hole and the island are circular. We also assume that the dynamics is diffusion-limited, as in Ref.<sup>11</sup>. From the assumption of fast adatom attachment-detachment kinetics at the island and hole edges, the concentrations are fixed to its equilibrium value. Hence, the concentrations are  $c_{eq}^A$  at the hole edge, and  $c_{eq}^B$  at the island edge. In such a geometry, the diffusion problem can be solved in bi-polar coordinates<sup>19</sup>. The adatom mass flux from the hole to the island is then found to be:

$$J = \frac{2\pi D \Delta c}{\ln[\pi d^2 / (AB)^{1/2}]}, \quad (4)$$

where  $\Delta c = c_{eq}^A - c_{eq}^B$ , and  $A$  and  $B$  are the areas of the hole and of the island, and  $d$  is the distance between the center of the hole and the center of the island. From mass conservation, the flux  $J$  is then related to the evolution of the hole area:

$$\partial_t A = \frac{\Omega}{h} J = \frac{2\pi \Omega D \Delta c}{h \ln[d^2 \pi / (AB)^{1/2}]}, \quad (5)$$

where  $\Omega = a^2$  is the atomic area. The hole and island areas are then related via global mass conservation

$$\partial_t B = h \partial_t A. \quad (6)$$

Since the island forms after the hole, we may assume that at  $t = 0$ ,  $A = A_0$  and  $B = 0$ , so that

$$A = \frac{B}{h} + A_0. \quad (7)$$

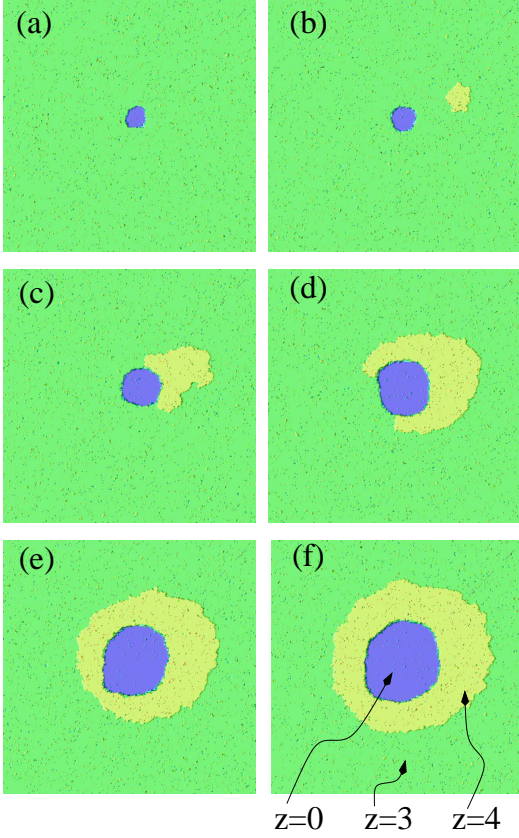


FIG. 2: Typical dynamics in the layer-by-layer dewetting regime. Parameters:  $T = 0.4$ ,  $E_S = 0.25$ , system size  $400 \times 400$ , and  $h = 3$ . (a) A hole is performed artificially in the film. (b) An island nucleates far from the hole. (c) Diffusion limited mass transfer from the hole to the island leads to the simultaneous growth of the island and the hole. (d) The monolayer island surrounds the hole. (e) The monolayer island closes around the hole and forms a monolayer rim. (f) The monolayer rim grows and becomes circular.

Using this relation into Eq.(5), we find:

$$\partial_t A = \frac{2\pi\Omega D\Delta c}{h \ln[d^2\pi/(hA(A - A_0))^{1/2}]} \quad (8)$$

the solution of which can be written in the implicit form:

$$\bar{A}_0 \ln \left[ \frac{\bar{A}_0}{\bar{A}} \right] - (\bar{A} - \bar{A}_0) \ln \left[ \frac{h}{e^2} \bar{A}(\bar{A} - \bar{A}_0) \right] = \frac{4\Omega D\Delta c}{hd^2} t, \quad (9)$$

where  $\bar{A} = A/\pi d^2$ , and  $\bar{A}_0 = A_0/\pi d^2$ . At long times, but when the hole is still small as compared to the hole-island distance, i.e. when  $1 \gg \bar{A} \gg \bar{A}_0$ , one has:

$$\bar{A} \ln \left[ \frac{e^2}{\bar{A}^2 h} \right] \approx \frac{4\Omega D\Delta c}{hd^2} t. \quad (10)$$

## B. Comparison to KMC simulations

In order to compare Eq.(9) with KMC simulations, we need to evaluate the parameters which enter in the model. We choose the lattice spacing as our unit length, and the time unit is the inverse of the attempt frequency. Hence  $\Omega = 1$  and  $\nu_0 = 1$ . Since an atom can move randomly to the 4 nearest neighbor sites, the diffusion constant on the film is  $D = 1/4$ . Moreover, we obtain the equilibrium concentration on the film  $c_{eq} = e^{-2J/T}$  from the detailed balance of attachment-detachment at kink sites. Since the curvature of the island is larger than the curvature of the critical island size, we may assume that the Gibbs-Thomson contributions proportional to the curvature, are negligible, and  $c_{eq}^B \approx c_{eq}$ .

The chemical potential in the vicinity of the film edge is  $E_S/Th$ , as shown in Appendix A. Our reference state is the state of equilibrium on top of the film, with equilibrium concentration  $c_{eq}$  (this is the equilibrium concentration in the vicinity of an atomic step on the top of the film). Using the standard formula:

$$\mu = T \ln \frac{c_{eq}^A}{c_{eq}}, \quad (11)$$

we find that

$$c_{eq}^A = c_{eq} e^{\mu/T} = c_{eq} e^{E_S/Th}. \quad (12)$$

We therefore have

$$\Delta c = e^{-2J/T} \left( e^{E_S/(hT)} - 1 \right). \quad (13)$$

Using these parameters, the solution of Eq.(9) is in good agreement with KMC simulations, as shown in Fig.3. Note that the Eq.(9) cannot lead to a perfect agreement with KMC simulations due to inherent assumptions of the model. Indeed, we have assumed that the island and hole are isolated, neglecting interaction with the periodic images of the island and the hole. In addition, the condition that the island-hole distance  $d$  is much larger than the radii of the hole and the island is verified at the beginning, but not at end of the KMC simulation. Finally, we observe in Fig.3 that the condition  $A \gg A_0$  is not verified in the KMC simulations. Therefore, the asymptotic linear solution (10) cannot provide a good approximation for the KMC simulations result.

## IV. GROWTH OF A MONOLAYER RIM AROUND A HOLE

### A. Model

Due to the smaller thickness of the monolayer as compared to that of the hole, the island area increases faster than that of the hole, as shown by Eq.(6). Once the island becomes large enough, it collides with the hole and

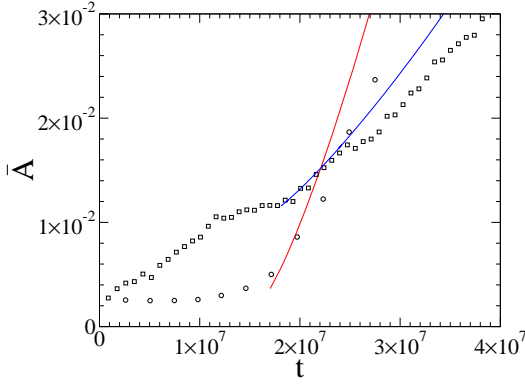


FIG. 3: Dynamics of one hole exchanging mass with a distant monolayer island. The symbols are the results of KMC simulations with:  $T, E_S, h = 0.4, 0.2, 2$  (squares), and  $0.35, 0.25, 2$  (circles), in a  $400 \times 400$  periodic lattice. (In order to fit both curves in the same plot, the timescale of the first data set (squares) was multiplied by 6). The solid lines represents the solution of Eq.(9) where the initial conditions and the value of  $d$  were measured from the simulations.

surrounds it. Then, a different regime can be observed, where the hole is surrounded by a monolayer rim. This monolayer rim is initially very far from being circular. However, the diffusion limited transport provides more mass to the parts of the monolayer rim which are closer to the hole, resulting in a stabilization of the rim, which becomes approximately circular. In this section, we present the exact solution of the circular rim evolution dynamics, and compare this solution to the asymptotic solution given in Ref.<sup>11</sup>.

Mass exchange occurs on top of the monolayer rim via adatom diffusion. The adatom concentration field on the rim obeys:

$$\frac{1}{r} \partial_r [r \partial_r c] = 0, \quad (14)$$

which has a solution of the form

$$c = c_0 \ln[r/r_0]. \quad (15)$$

We once again assume instantaneous attachment-detachment kinetics, so that  $c = c_1$  at  $r = R_1$  at the edge of the hole and  $c = c_2$  at  $r = R_2$  at the other edge. Moreover, we must impose mass conservation

$$\begin{aligned} \partial_t R_2 &= -\frac{\Omega}{h_2} D \partial_r c|_2, \\ \partial_t R_1 &= -\frac{\Omega}{h_1} D \partial_r c|_1, \end{aligned} \quad (16)$$

where  $h_1 = h + 1$  is the rim height, and  $h_2 = 1$  is the thickness of the monolayer rim. Introducing the areas  $A_1 = \pi R_1^2$  and  $A_2 = \pi R_2^2$ , we find

$$\partial_t A_1 = \frac{4\pi D \Omega \Delta c}{h_1 \ln[A_2/A_1]}, \quad (17)$$

where  $\Delta c = c_1 - c_2$  is given by Eq.(13) with the substitution  $h \rightarrow h_1$ . The evolution of  $A_2$  is fixed by the mass conservation relation

$$h_2 \partial_t A_2 = h_1 \partial_t A_1, \quad (18)$$

which implies

$$A_2 = \frac{h_1}{h_2} (A_1 - A_1^0) + A_2^0, \quad (19)$$

where  $A_i^0$  are the areas at  $t = 0$ . Substituting this expression for  $A_2$  into Eq.(17), one finds the solution in an implicit form:

$$\begin{aligned} &h_2 (A_2 \ln[A_2] - A_2^0 \ln[A_2^0]) \\ &- h_1 (A_1 \ln[A_1] - A_1^0 \ln[A_1^0]) \\ &= 4\pi D \Omega \Delta c t. \end{aligned} \quad (20)$$

At large times when  $A_1 \gg A_1^0$  and  $A_2 \gg A_2^0$ , we find

$$\begin{aligned} A_1 h_1 \ln \left[ \frac{h_1}{h_2} \right] + A_1^0 h_1 \ln \left[ \frac{A_1^0 h_2}{e A_1 h_1} \right] - A_2^0 h_2 \ln \left[ \frac{A_2^0 h_2}{e A_1 h_1} \right] \\ \approx 4\pi D \Omega \Delta c t. \end{aligned} \quad (21)$$

Keeping the dominant terms only, we obtain a linear behavior at large times

$$A_1 \approx \frac{4\pi D \Omega \Delta c}{h_1 \ln[h_1/h_2]} t \quad (22)$$

which is the asymptotic form presented in Ref.<sup>11</sup>.

## B. Comparison to KMC simulations

In Fig4, we have compared the KMC simulations results with Eq.(20) and Eq.(22). The agreement between the linear asymptotic formula (22) and KMC simulations results requires a fitting parameter (e.g. the reference time for which  $A_1^0$  extrapolates to zero). However, due to the divergence of the subdominant terms in Eq.(21), the meaning of this parameter is unclear.

Therefore, it is more satisfactory to use the full solution (20). Indeed, the full solution requires no fitting parameter: we simply need to measure  $A_1^0$  and  $A_2^0$  at an initial time once the monolayer rim is formed. The full solution is shown to be in good agreement with the KMC simulations in Fig.4.

## V. ZIPPING OF A MONOLAYER ON A FACETTED RIM

We now turn to another regime, which appears for large  $E_S$  and small  $h$ . In this regime, a thick multilayer rim forms. The top of this rims is faceted. The increase of the rim height proceeds via the nucleation of monolayer islands on the rim facet. Once they are nucleated, these islands grow in size so as to invade the whole rim facet, as shown on Fig.5. Here, we want to focus on the growth process of the monolayer islands.

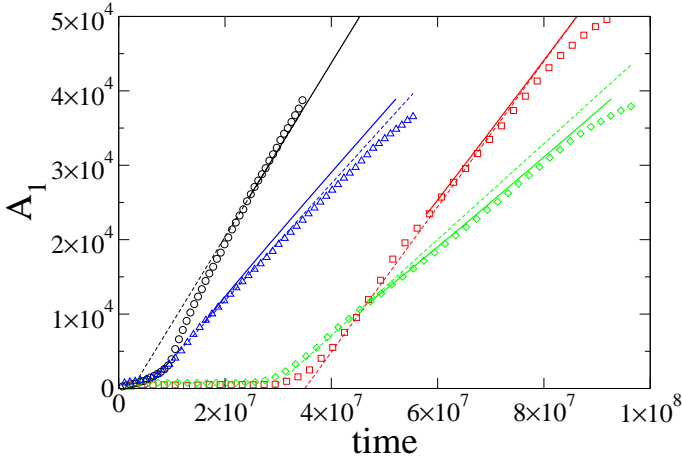


FIG. 4: Diffusion limited regime. Dynamics of  $A_1$  for a hole with a monolayer rim. The dashed lines correspond to the asymptotic linear formula Eq.(22). The solid lines correspond to the full solution Eq.(20) without fitting parameter.

### A. Monolayer zipping velocity

Let us consider a straight dewetting front of height  $h_1$ , with a rim facet of width  $\ell = x_2 - x_1$ . We aim to analyze the velocity of an island zipping along the dewetting front. We assume that the dewetting front does not deform and remains straight during this process. The driving force for the atoms to detach from the front, and to attach to the monolayer step is the difference between the chemical potential of the straight film edge  $E_S/h_1$  (see Appendix A), and the chemical potential of the step  $\Omega\tilde{\gamma}\kappa$ , leading to:

$$\Delta\mu = \frac{E_S}{h_1} - \Omega\tilde{\gamma}\kappa, \quad (23)$$

where  $\kappa$  is the step curvature, and  $\tilde{\gamma}$  is the step stiffness. Here it is assumed that the temperature is high enough so that steps properties are isotropic. As a consequence, we have  $\tilde{\gamma} \approx \gamma$ .

The mobility of the atoms for diffusion between the film edge and the atomic step is  $M = Dc_{eq}/(\lambda T)$ , where  $\lambda$  is the typical distance between the fronts. The only available geometric scale for a monolayer rim zipping along a dewetting front is the step curvature, and we therefore expect  $\kappa \sim 1/\lambda$ .

As a summary, the zipping velocity should take the form:

$$V_{zip} = M\Delta\mu \sim \frac{\Omega Dc_{eq}}{T} \kappa \left( \frac{E_S}{h_1} - \Omega\gamma\kappa \right). \quad (24)$$

We assume that the selected curvature is the one which maximizes the velocity:

$$\kappa = \frac{E_S}{2h_1\Omega\gamma}. \quad (25)$$

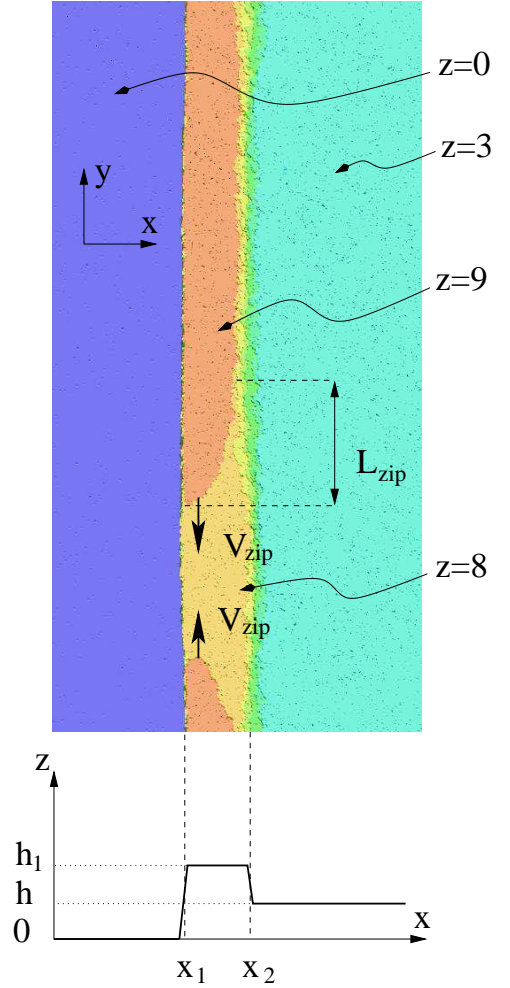


FIG. 5: Zipping of a monolayer island on the rim facet. Detail of a KMC simulation on a  $1000 \times 1000$  lattice with  $T = 0.4$ ,  $E_S = 0.5$ ,  $h = 3$ . On this image,  $h_1 = 8$ .

Thus, the zipping velocity takes the form

$$V_{zip} \approx C_{zip} \frac{Dc_{eq}E_S^2}{Th_1^2\gamma}, \quad (26)$$

where  $C_{zip}$  is an unknown number.

### B. Time for the top step to cross the rim facet

Two-dimensional islands are usually nucleated close to the front  $h_1$ . The islands grow in the  $y$  direction with velocity  $V_{zip}$ , as discussed in the previous subsection. But islands also grow in the  $x$  direction. In order to model the growth in the  $x$  direction we use a 1D model, where a step is parallel to the front. This 1D model only makes sense in the limit of small slopes  $\partial_y x \ll 1$ . We assume that dynamics is limited by diffusion on the top of the monolayer island. The chemical potential difference between the dewetting front and the island edge is  $E_S/(h_1 + 1)$ .



Assuming once again fast attachment-detachment kinetics, the concentration at the step edge and at the front edge are respectively  $c_{eq}$ , and  $c_{eq} \exp[E_S/(h_1+1)T]$ . The concentration profile is therefore linear, and the flux per unit length from the front to the island edge is:

$$J = \frac{Dc_{eq}}{x_s} \left( e^{E_S/(h_1+1)T} - 1 \right), \quad (27)$$

where  $x_s$  is the distance between the dewetting front and the island edge. The velocity of the island edge in the  $x$  direction is therefore:  $dx_s/dt = \Omega J$ . From this equation, we find

$$x_s = \left[ 2\Omega Dc_{eq} \left( e^{E_S/(h_1+1)T} - 1 \right) t \right]^{1/2}. \quad (28)$$

The step will reach the step bunch at  $x_s = \ell$  in a time  $t_\ell$ . For weak driving forces,  $E_S \ll Th_1$ , one has

$$t_\ell = \frac{\ell^2}{2\Omega Dc_{eq}} (h_1 + 1) \frac{T}{E_S}. \quad (29)$$

### C. Zipping length

The direct observation of  $V_{zip}$  or  $t_\ell$  in the KMC simulations would require delicate front tracking procedures and we shall look for a quantity which can be observed on a single snapshot. From relation (29), the tip length of the zipping monolayer reads:

$$L_{zip} = V_{zip} t_\ell \approx C_{zip} \frac{E_S}{2\Omega\gamma} \ell^2 \frac{h_1 + 1}{h_1^2}. \quad (30)$$

The length  $L_{zip}$  is the length between the tip of the zipping monolayer (in the vicinity of the front of height  $h_1$ ), and the point where the step edge of this monolayer reaches the bunch of height  $h_2$  (the distance is measured along  $y$ ).

Since the nucleation barrier for the formation of new monolayer islands grows with  $h_1$ , the typical distance between island nucleation sites increases exponentially with  $h_1$ , as shown in Ref.<sup>11</sup>. Thus, the length  $L_{zip}$  is always smaller than the typical distance between island nucleation sites. Therefore, for large enough  $h_1$ , the islands first reach the total width  $\ell$  of the facet, and then zip along the dewetting front with a tip length  $L_{zip}$ . This is indeed the scenario observed in KMC simulations.

### D. Comparison to KMC

We have performed KMC simulations, with  $E_S = 0.5$ ,  $T = 0.4$ ,  $h = 3$ , in a  $1000 \times 1000$  system with total simulation time  $t = 3.5 \times 10^8$ . The simulation time is chosen to be large enough for the system to reach the late stage regime where  $L_{zip} \gg \ell$ . Measurements were performed on five KMC simulations snapshots, each time measuring  $L_{zip}$  from an average of its value at the two

$h_1$	$\ell$	$L_{zip}$	$C_{zip}$
6	56	86	0.24
6	56	54	0.15
7	69	150	0.31
7	85	180	0.24
8	83	124	0.20

TABLE I: Observed values of  $\ell$  and  $L_{zip}$  from KMC simulations with  $T = 0.4$ ,  $E_S = 0.5$ , and  $h = 3$  in a  $1000 \times 1000$  lattice.

ends of the expanding island on the top facet. From each measurement, we have extracted the value of  $C_{zip}$  from Eq.(30) with  $\gamma = 0.42^{10,11,20}$ . The results are reported in Table I. We obtain the average value

$$C_{zip} \approx 0.25 \pm 0.05. \quad (31)$$

The error here provides an indication of the order of magnitude for the observed variations of  $C_{zip}$  extracted from different measurements. The result (31) does not include the case where  $h_1 = 6$ , for which the condition  $\ell \ll L_{zip}$  is not verified. Nevertheless, we see in Table I that the results with  $h_1 = 6$  would provide similar values for  $C_{zip}$ .

Finally, we would like to point out that we have not yet studied systematically all possible regimes of zipping, due to limitations in the our KMC simulations. Indeed, for smaller values of  $E_S$ , the simulation time is too large, and for larger values of  $E_S$ , the solid on solid restriction (which forbids overhangs) should be released. Important improvements in our numerical approach are therefore needed in order to address these questions.

## VI. CONCLUSION

In conclusion, we have analyzed the motion of atomic steps during the dewetting of ultra-thin solid films with various geometries: (i) simultaneous growth of a monolayer island with a hole; (ii) expansion of a hole with a monolayer rim; (iii) zipping of a monolayer island on the top facet of a thick rim.

Our KMC results are in good agreement with step models where mass transport is limited by diffusion on terraces between steps. These results demonstrate that the step model approach provides a systematic way to investigate the evolution dynamics of thin films during the dewetting process.

Several additional ingredients could be added to the step models, such as anisotropy, non-trivial attachment-detachment kinetics (e.g. an Ehrlich-Schwoebel barrier, or step transparency), or elastic interactions between steps. We hope to report along these lines in the future.

We acknowledge support from "nanomorphogénèse" and "DéFiS" ANR-PNANO grants.

## Appendix A: Local chemical potential at the edge of a faceted film

The total free energy of a film of height  $h_0$  at  $x > x_0(y)$  (the height is zero at  $x < x_0(y)$ ) is:

$$\mathcal{F} = \int ds_0 \gamma_{edge} - E_S \Omega^{-1} \int dy x_0(y), \quad (\text{A1})$$

where  $s_0$  is the arclength along the edge of the film, and  $\gamma_{edge}$  is the free energy per unit length of the edge of the film. The total number of atoms in the film is:

$$\mathcal{N} = \mathcal{N}_0 - \Omega^{-1} h_0 \int dy x_0(y), \quad (\text{A2})$$

where  $\mathcal{N}_0$  is a constant. Equilibrium reads:

$$\delta(\mathcal{F} - \mu \mathcal{N}) = 0. \quad (\text{A3})$$

Our variable here is  $x_0(y)$ , the position of the edge. We therefore have:

$$\mu = \frac{\delta \mathcal{F}}{\delta x_0(y)} \left( \frac{\delta \mathcal{N}}{\delta x_0(y)} \right)^{-1}. \quad (\text{A4})$$

Using the above expressions:

$$\mu = \Omega \tilde{\gamma}_0 \kappa_0 + \frac{E_S}{h_0}, \quad (\text{A5})$$

where  $\tilde{\gamma}_0 = (\gamma_{edge} + \gamma''_{edge})/h_0$  is the stiffness per layer of the film edge (If the edge is a bunch of steps, and if the step-step interaction is negligible, then  $\tilde{\gamma}_0$  is the step stiffness). Note that this derivation of the chemical potential relies on the postulate that the film profile across the film edge does not vary along along the film edge.

- 
- <sup>1</sup> C. Misbah, O. Pierre-Louis, and Y. Saito, Rev. Mod. Phys. (2009).
  - <sup>2</sup> W. K. Burton, N. Cabrera, and F. C. Frank, Phil. Trans. Roy. Soc. London, A, **243**, 299 (1951).
  - <sup>3</sup> A. Chame, S. Rousset, H. Bonzel, and J. Villain, Bulg. Chem. Commun. **29**, 398 (1996).
  - <sup>4</sup> M. Khenner, Physical Review B (Condensed Matter and Materials Physics) **77**, 245445 (pages 6) (2008), URL <http://link.aps.org/abstract/PRB/v77/e245445>.
  - <sup>5</sup> W. Kan and H. Wong, J. Appl. Phys. **97**, 043515 (2005).
  - <sup>6</sup> H. Wong *et al*, Acta Mater **48**, 1719 (2000).
  - <sup>7</sup> M. Khenner, Phys. Rev. B **77**, 165414 (2008).
  - <sup>8</sup> J.-N. Aqua, T. Frisch, and A. Verga, Physical Review B (Condensed Matter and Materials Physics) **76**, 165319 (pages 5) (2007), URL <http://link.aps.org/abstract/PRB/v76/e165319>.
  - <sup>9</sup> D. Srolovitz and S. Safran, J. Appl. Phys. **60**, 255 (1986).
  - <sup>10</sup> O. Pierre-Louis, A. Chame, and Y. Saito, Phys Rev Lett **99**, 136101 (2007).
  - <sup>11</sup> O. Pierre-Louis, A. Chame, and Y. Saito, Physical Review Letters **103**, 195501 (pages 4) (2009), URL <http://link.aps.org/abstract/PRL/v103/e195501>.
  - <sup>12</sup> K. Thürmer, E. D. Williams, and J. E. Reutt-Robey, Physical Review B (Condensed Matter and Materials Physics) **68**, 155423 (pages 7) (2003), URL <http://link.aps.org/abstract/PRB/v68/e155423>.
  - <sup>13</sup> B. Yang and et al, Phys. Rev. B **72**, 235413 (2005).
  - <sup>14</sup> E. Dornel, J.-C. Barbé, G. Lacolle, and J. Eymery, Phys. Rev. B **73**, 115427 (2006).
  - <sup>15</sup> M. Coll *et al*, Physical Review B **73**, 075420 (2006).
  - <sup>16</sup> M. Kotrla, Computer Physics Communications **97**, 82 (1996).
  - <sup>17</sup> P. G. de Gennes, Reviews of Modern Physics **57**, 827 (1985), URL <http://link.aps.org/abstract/RMP/v57/p827>.
  - <sup>18</sup> R. Sangiorgi, M. Muolo, D. Chatain, and N. Eustathopoulos, J. Am. Ceram. Soc. **71**, 742 (1988).
  - <sup>19</sup> P. Morse and F. H., *Methods of Theoretical Physics* (McGraw-Hill, New York, 1953).
  - <sup>20</sup> B. Krishnamachari *et al*, Phys. Rev. B **54**, 8899 (1996).